The Astrophysical Journal, 904:122 (10pp), 2020 December 1 https://doi.org/10.3847/1538-4357/abbe21

Whether Small Flux Ropes and Magnetic Clouds Have the Same Origin: A Statistical Study of Small Flux Ropes in Different Types of Solar Wind

Mengjiao Xu[1,2], Chenglong Shen[1,2], Qiang Hu[3], Yuming Wang[1,2,4], and Yutian Chi[1,2,5]
[1] CAS Key Laboratory of Geospace Environment, Department of Geophysics and Planetary Sciences, University of Science & Technology of China, Hefei, Anhui 230026, People's Republic of China; clshen@ustc.edu.cn
[2] CAS Center for Excellence in Comparative Planetology, University of Science and Technology of China, Hefei, People's Republic of China
[3] Department of Space Science and CSPAR, The University of Alabama in Huntsville, Huntsville, AL 35805, USA
[4] Mengcheng National Geophysical Observatory, School of Earth and Space Sciences, University of Science and Technology of China, Hefei 230026, People's Republic of China
[5] Department of Meteorology, University of Reading, Berkshire, UK
Received 2020 July 22; revised 2020 September 26; accepted 2020 September 29; published 2020 November 26

Abstract

According to the duration and size, magnetic flux ropes can be divided into large-scale flux ropes, namely, magnetic clouds, and small-scale flux ropes (SFRs). Whether SFRs have the same origin as magnetic clouds has been a hot topic for a long time. Based on the SFR database developed by Hu et al. and Chen et al., this paper analyzes the properties of SFRs in different types of solar wind, which are SFRs in interplanetary coronal mass ejections (ICMEs), SFRs in stream interaction regions, and SFRs in background solar wind. On the assumption that SFRs in ICMEs have the same origin as magnetic clouds, we compare the three types of SFRs from several aspects, attempting to shed some light on the dispute, i.e., whether SFRs are homologous to magnetic clouds. The results show that up to 91% of the SFRs are outside ICMEs. Unlike SFRs in ICMEs, SFRs outside ICMEs seldom have large magnetic field strength and apparent expansion signatures. In addition, 36% of the SFRs in ICMEs have enhanced iron charge states. This probability is much higher than the other two types of SFRs. By an automatic method, this paper also find that counterstreaming electrons are more common in SFRs in ICMEs. Considering strong magnetic field, expansion signatures, large iron charge state, and counterstreaming electrons are important indicators of magnetic clouds, we believe that most of the SFRs near Earth have different origins from magnetic clouds.

Unified Astronomy Thesaurus concepts: Interplanetary magnetic fields (824); Solar wind (1534); Solar coronal mass ejections (310)

1. Introduction

Magnetic flux ropes are structures of twisted magnetic field, threaded along an axis. According to the duration time and scale size, magnetic flux ropes can be further divided into large-scale flux ropes and small-scale flux ropes (SFRs). Large-scale flux ropes, known as magnetic clouds (MCs), have a typical duration of 1 day and a typical diameter of 0.2–0.4 au (e.g., Lepping et al. 1990). MCs are a subset of interplanetary coronal mass ejections (ICMEs), with the signatures of enhanced magnetic field strength, large and smooth magnetic field rotation, as well as low plasma temperature and β (e.g., Burlaga et al. 1981; Cane & Richardson 2003; Jian et al. 2006). SFRs are first introduced by Moldwin et al. (1995) and Moldwin et al. (2000). Basically, they last no more than 12 hr and have diameters less than 0.2 au (Feng et al. 2007).

In the past two decades, people have carried out a lot of research that focused on the solar sources, characteristics and geomagnetic effects of MCs, but the research on SFRs is not adequate. To date, the origin of SFRs is still controversial. Or rather, whether MCs and SFRs have the same origin remains to be investigated. Moldwin et al. (2000) claimed that SFRs are caused by the magnetic reconnection at the heliospheric current sheet (HCS) because of the lack of intermediate-scale magnetic flux ropes between MCs and SFRs. They speculated that if SFRs and MCs are of the same physical origin, then the magnetic flux ropes should have a continuous size distribution. This was further confirmed by Cartwright & Moldwin (2008) and Janvier et al. (2014a), who showed that the distribution of the flux rope duration is double peaked: the radii of SFRs present a steep power-law distribution, while the radii of MCs present a Gaussian distribution. In contrast, through analyzing the Wind observation from 1995 to 2001, Feng et al. (2007) proposed that magnetic flux ropes have a continuous size distribution. Hence, they deemed that SFRs are interplanetary manifestations of small coronal mass ejections (CMEs). Apart from their sizes, there are many other disputes. For example, unlike MCs, little expansion effect can be directly observed by in situ measurements for SFRs (Feng et al. 2007; Cartwright & Moldwin 2008; Yu et al. 2014). However, Janvier et al. (2014b) attributed the difference to the hidden of the SFRs' expansion characteristics by the velocity fluctuations. In addition, in some research, the occurrence rate of small-scale magnetic flux ropes was discovered to have a negative solar-cycle dependency (Cartwright & Moldwin 2010; Yu et al. 2014, 2016; Nieves-Chinchilla et al. 2019), which was opposite to the solar-cycle variance of the MCs' frequency. On the contrary, Feng et al. (2008) found a positive correlation between the occurrence rates of SFRs and MCs from 1995 to 2005. One obvious caveat of these studies is that they all suffer from relatively small sample sizes. Based on an automated detection algorithm, Hu et al. (2018) showed the statistical properties of tens of thousands SFRs. Their results indicated a continuous distribution of duration and scales sizes, and a positive correlation between the occurrence rate and sunspot numbers.

Since the SFRs can be affected by the solar wind during the propagation, it is a wise choice to eliminate the propagation effects in order to better understand the origin of SFRs (Janvier et al. 2014b; Feng & Wang 2015). Fortunately, the charge states of the ion are frozen in the interplanetary space (Buergi & Geiss 1986; Song & Yao 2020). Average iron charge states ($\langle Q_{\rm Fe}\rangle$) in the solar wind are typically around 9–11 (Lepri et al. 2001). Usually, the appearance of high ionic charge states ($\langle Q_{\rm Fe}\rangle$ >12) represents the high temperature caused by magnetic reconnection in the flare region (e.g. Bemporad et al. 2006; Ko et al. 2013; Song et al. 2015; Huang et al. 2018). Therefore, the high Fe charge state is a reliable ICME indicator, which has been observed in more than 50% of ICMEs (Lepri & Zurbuchen 2004). Inspired by this, Feng & Wang (2015) investigated the iron charge states in SFRs, finding that half of the SFRs have high iron charge states. This implied that SFRs and MCs may have the same origin. However, by investigating the variations of $\langle Q_{\rm Fe}\rangle$ in small transients, Yu et al. (2016) demonstrated that $\langle Q_{\rm Fe}\rangle$ only increased in less than 5% of small transients.

In addition to the high charged states, obvious counter-streaming suprathermal electrons (CSEs) are also characteristic of ICMEs. CSEs can be interpreted as indication of closed magnetic field lines, with both ends connected to the Sun (e.g., Larson et al. 1997). Feng et al. (2015) investigated the CSE signatures of 106 SFRs measured by Wind during 1995–2005, finding that 75% of the 106 flux ropes contain CSEs, and the percentages of CSE duration vary from 8% to 98%, with a mean value of 51%. Also, the SFRs far from the HCS have more obvious signatures of CSEs than the SFRs in the vicinity of the HCS. However, the CSE intervals were recognized by naked eye in that work, which may be less objective.

As we have mentioned before, the origin of SFRs is still debatable. Underlying these controversies presented above is the fact that the SFRs analyzed by different studies vary widely. People have a disparate comprehension of the standard set of criteria for identifying SFRs. Besides, the total numbers of SFR events in most of the studies are far too few. The more convincing statistical results rely on an integral and accurate SFR database. Recently, Hu et al. (2018) developed a new automated small-scale magnetic flux rope detection algorithm based on the Grad–Shafranov (GS) reconstruction technique (see Hu 2017 for a comprehensive review). This program was first applied to the Wind observation from 1996 to 2016, and successfully detected a total number of 74,241 SFRs with a duration from 9 to 361 minutes. Following this work, Chen et al. (2019) established the SFR database based on the measurements of Advanced Composition Explorer (ACE) spacecraft, which is publicly available at http://fluxrope.info, and they have extended the upper limit of flux rope duration to 36 hr. To some extent, the ACE event database might be better than the Wind database since they have extended the upper limit of flux rope duration to tens of hours, which would accommodate some large-scale flux ropes. Although the ACE SFRs can be as long as 36 hr, only about 1‰ of them are longer than 12 hr, which satisfies the commonly accepted timescale of SFRs. We acknowledge that some long-duration SFRs are no longer small scale in size. Considering that these events are few and far between, which means that the statistical properties of SFRs with a duration less than 12 hr will dominate the interpretation of our results, we still use this terminology for consistency. In other words, some SFRs may coincide with alternatively identified ICMEs in other studies. They fall into the category $\rm SFRs_{ICME}$ as described below. In this work, we will analyze the ACE-observed SFRs detected by this automated algorithm in this work.

This paper is organized as follows. In Section 2, we will classify the SFRs listed in the ACE SFR database into three groups, according to the solar wind type they reside in. They are SFRs in ICMEs ($\rm SFRs_{ICME}$), SFRs in SIRs ($\rm SFRs_{SIR}$), and SFRs in background solar wind ($\rm SFRs_{SW}$). Supposing $\rm SFRs_{ICME}$ have the same origin as MCs, we will analyze the difference between $\rm SFRs_{ICME}$ and the other two groups of SFRs in Section 3, trying to discern the origins of $\rm SFRs_{SIR}$ and $\rm SFRs_{SW}$. In this section, we will compare the three groups of SFRs from the perspectives of the distribution of basic parameters, iron charge state and CSEs. Section 4 will summarizes our findings and briefly discuss the origination of SFRs based on our results.

2. Classification of Small Flux Ropes

In this work, we use the ACE data to analyze the properties of SFRs in different types of solar wind from 1998 to 2015. The SFRs studied in this paper are from the SFR database established by Hu et al. (2018) and Chen et al. (2019), which gives the small flux ropes identified via Wind observation from 1996 to 2016, the small flux ropes identified via ACE observation from 1998 to 2018 and the small flux ropes identified via Ulysses observation from 1991 to 2009. The small flux ropes in this database are detected by an automated program based on the GS reconstruction algorithm. The online database can be found at http://fluxrope.info. In the following work, we will classify the SFRs observed by ACE according to the type of solar wind they are located in, and analyze the characteristics and differences of SFRs in different types of solar wind.

Stream interaction regions (SIRs) and ICMEs are two kinds of large-scale structures in the interplanetary space, which have different characteristics from the background solar wind. SIRs are caused by the interactions between the fast solar wind streams and slow solar wind streams. The compressed proton number density, total pressure, and magnetic field at the interface together with the continuously increasing solar wind speed are the main characteristics used to identify possible SIRs. ICMEs are the interplanetary counterparts of CMEs, showing a number of signatures including enhanced magnetic field strength, large and smooth magnetic field rotation, low proton temperature, low plasma β, high iron charge state, and obvious counterstreaming electrons. These characteristics reflect different physical mechanisms that CMEs experience during the eruption and propagation process. For example, the high charge state of iron comes from the flare-related heating during the eruption; the reduced proton temperature stems from the ICME expansion during the propagation; and the obvious counterstreaming electrons represent that the feet of ICMEs are connected to the solar surface. Since not all CMEs go through the same physical processes, most CMEs have only a few of these characteristics. With these criteria, Chi et al. (2016) and Chi et al. (2018) set up catalogs of 427 ICMEs and 620 SIRs during the period from 1998 to 2015 using the in situ observations, respectively.

Based on the existing ICME and SIR catalogs, we can divide the near-Earth in situ spacecraft observations in interplanetary space into three types: ICMEs, SIRs, and background solar

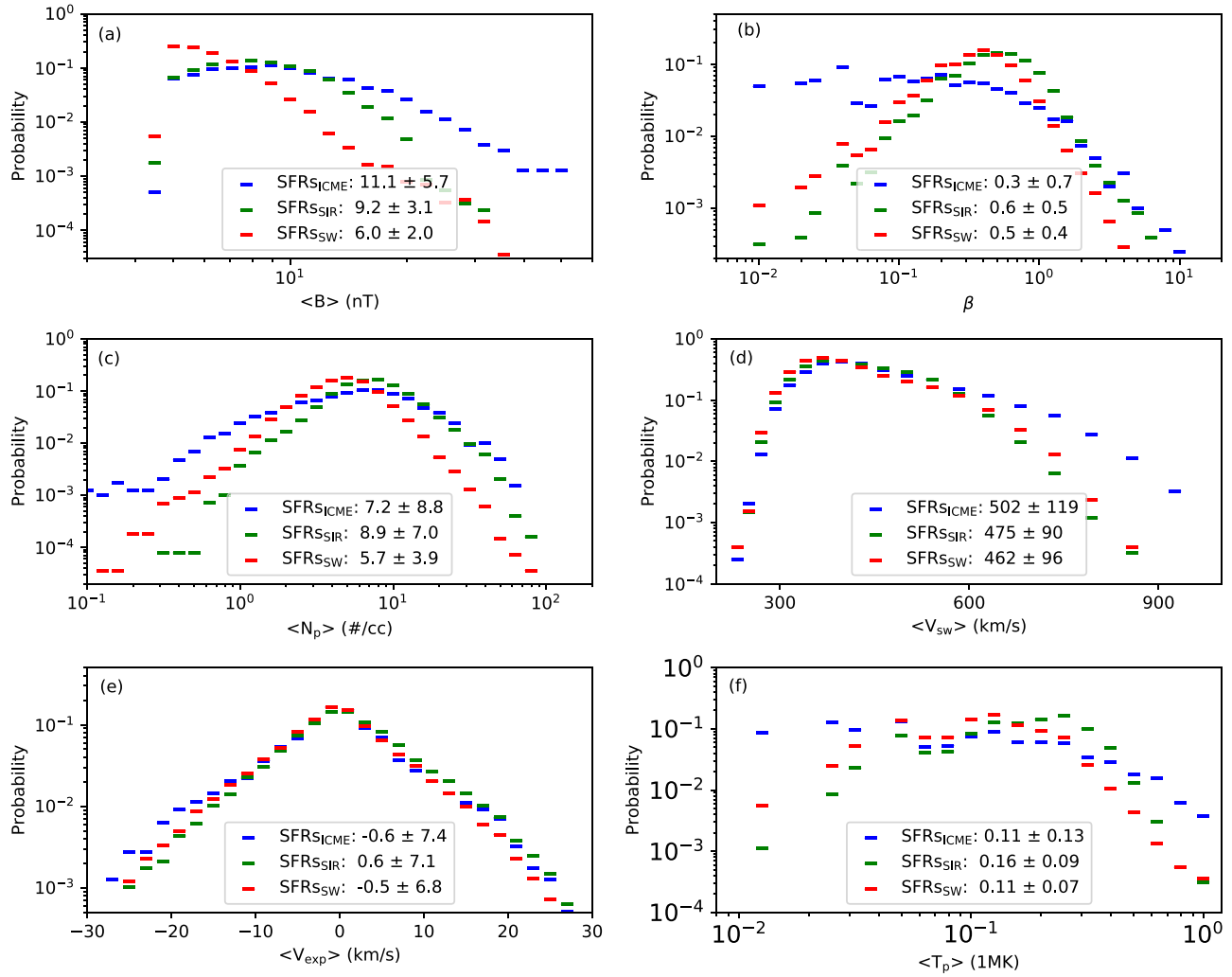

Figure 1. Parameter distributions of small-scale flux ropes in different types of solar wind. The blue, green, and red markers denote $SFRs_{ICME}$, $SFRs_{SIR}$, and $SFRs_{SW}$, respectively. (a) The averaged magnetic field strength. (b) The averaged proton β. (c) The averaged proton number density. (d) The averaged solar wind speed. (e) The expansion velocity. (f) The averaged proton temperature.

wind. And then, the SFRs observed by ACE can be classified into three groups according to the type of interplanetary space in which they reside, namely, SFRs in ICMEs ($SFRs_{ICME}$), SFRs in SIRs ($SFRs_{SIR}$), and SFRs in background solar wind ($SFRs_{SW}$). During the period from 1998 to 2015, 45,127 SFRs are determined by the ACE observation, of which 3977 are located in ICMEs (2415 in ejeta and 1562 in sheath regions), 12,700 are located in SIRs and 27,769 are located in background solar wind. The other 681 SFRs cross two different types of solar wind, which means that the front boundaries and the rear boundaries of the SFRs are located in different types of solar wind. This may be due to uncertainties in the definition of SIR or ICME boundaries, since all these ICME and SIR events are selected by the naked eye and their boundaries are generally hard to identify accurately. For the SFRs that cross two different types of solar wind, it is difficult to define the type of solar wind they really belong to. For simplicity, we just ignore those events. So these are removed from our analysis. The numbers of $SFRs_{ICME}$, $SFRs_{SIR}$, and $SFRs_{SW}$ account for 9%, 29%, and 62%, respectively. We speculate that $SFRs_{ICME}$ originate from the solar eruptions, having the same origin as MCs, except that the automated detection of SFRs and the identification of MCs focus on different timescales, and some of the MCs are eroded to be small in scale during the propagation. Notably, however, $SFRs_{ICME}$ make up less than one-tenth of the total SFRs. Most of the SFRs are in SIRs or background solar wind. So what are the origins of these SFRs? Are they actually of the same origin as MCs, with relatively small sizes? To answer this question, we will compare the properties of $SFRs_{ICME}$ with $SFRs_{SIR}$ and $SFRs_{SW}$ in the following section.

3. Comparison of Small Flux Ropes in Different Types of Solar Wind

3.1. Properties of SFRs

Figure 1 presents the distributions of various parameters of $SFRs_{ICME}$, $SFRs_{SIR}$, and $SFRs_{SW}$ (blue, green, and red markers, respectively), including the proton number density, proton temperature, magnetic field strength, proton β, solar wind speed, and the expansion speed. The mean values and the standard deviations for the three types of SFRs are also listed in each panel.

From Figures 1(a) and (b), we can find that $SFRs_{ICME}$ have relatively large magnetic field strength and small plasma β. About 18% of $SFRs_{ICME}$ have averaged magnetic field strength

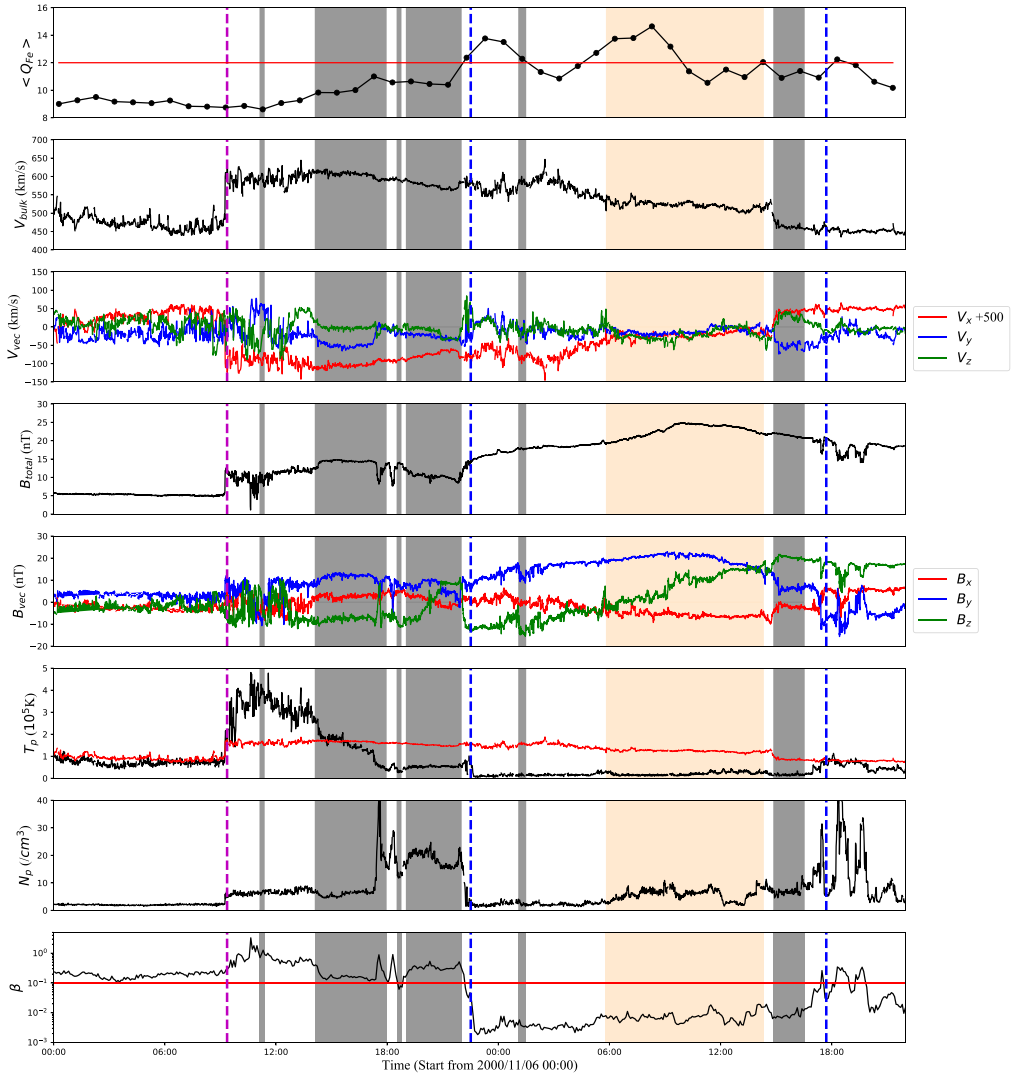

Figure 2. An example of the SFR with high $Q_{\rm Fe}$ on 2000 November 7. From the top to the bottom, the panels are the averaged iron charge state ($\langle Q_{\rm Fe}\rangle$), the bulk speed of the solar wind ($V_{\rm bulk}$), *x, y, z* components of the solar wind speed (V_x, V_y, V_z) in GSE coordinates, the magnitude of the total magnetic field ($B_{\rm total}$), *x, y, z* components of the magnetic field (B_x, B_y, B_z) in GSE coordinates, proton temperature ($T_{\rm p}$), proton density ($N_{\rm p}$), and proton β. The orange shaded region represents the studied SFR. The gray shaded regions represent the other SFRs in the ICME event. The violet vertical dashed line is the shock time, and the following two blue vertical dashed lines mark the ICME interval.

larger than 15 nT, compared with 5% and 1% of $\rm SFRs_{SIR}$ and $\rm SFRs_{SW}$. In addition, the probabilities of proton $\beta < 0.1$ for $\rm SFRs_{ICME}$, $\rm SFRs_{SIR}$, and $\rm SFRs_{SW}$ are 39%, 2%, and 4%, respectively. Figure 1(c) indicates that $\rm SFRs_{ICME}$ are more likely to be low density. Only 2‰ and 9‰ of $\rm SFRs_{SIR}$ and $\rm SFRs_{SW}$ have a proton density lower than 1, while for $\rm SFRs_{ICME}$, this ratio is 5%. All types of SFRs are more likely to travel at the speeds of the slow solar wind (300–600 km $\rm s^{-1}$), as can be seen from panel (d).

Figure 1(e) shows the distribution of expansion speed, which is half of the speed difference between the front and rear boundary of the SFR. As we can see here, few of these three types of SFRs have significant expansion velocity. However, the expansion velocity depends strongly on how big the studied structure is. For most of the SFRs in this study, the duration is less than 1 hr, so they are expected to have intrinsically small expansion velocity. Meanwhile, Janvier et al. (2014b) pointed out that the typical velocity fluctuation level observed in SFRs is relatively larger than the expansion velocity, which means that the expansion of most SFRs is masked by the velocity fluctuations. Therefore, for small magnetic flux ropes, the apparent expansion velocity may not be a good indicator of the expansion characteristics. On the other hand, the occurrences of solar wind plasma with abnormally low proton temperatures (*T*p) have long been considered a signature of expansion (Richardson & Cane 1995). Figure 1(f) shows that SFRs in background solar wind and SIRs seldom show the characteristics of very low temperature. For $\rm SFRs_{SIR}$ and $\rm SFRs_{SW}$, the probability of the averaged proton temperature falling below 30,000 K is 1% and 3%, respectively. Whereas for $\rm SFRs_{ICME}$, the probability can be as high as 22%. So in this regard, we believe that the expansion characteristics of $\rm SFRs_{SIR}$ and $\rm SFRs_{SW}$ are not as obvious as $\rm SFRs_{ICME}$.

Through analyzing the properties of SFRs in different types of solar wind, we find that unlike SFRs in ICMEs, SFRs outside ICMEs seldom show the characteristics of MCs, such as large magnetic field strength, low proton β, and obvious expansion. From this perspective, $\rm SFRs_{SIR}$ and $\rm SFRs_{SW}$ are unlikely to originate from the solar eruptions.

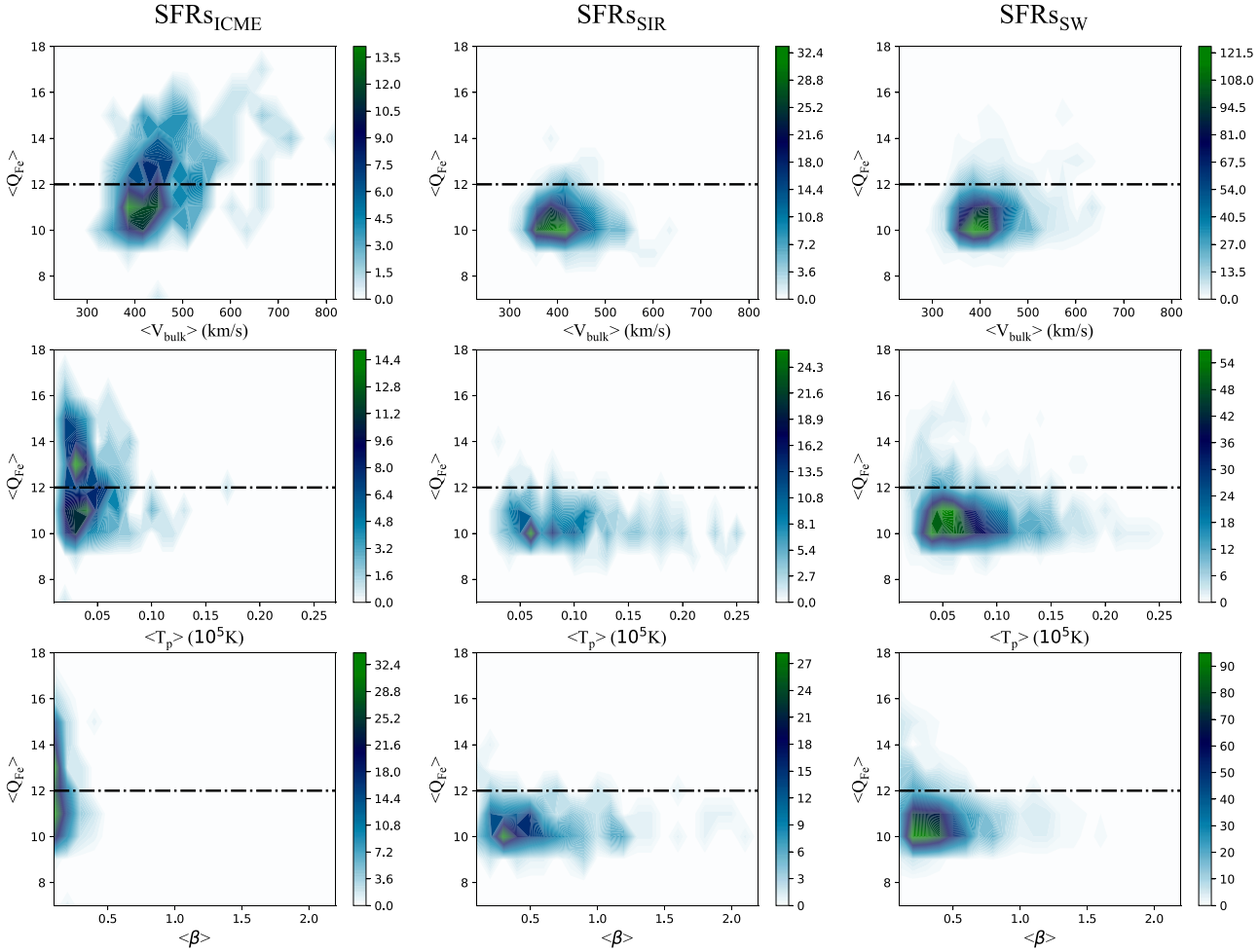

Figure 3. The two-dimensional distribution mean value of $\langle Q_{\rm Fe}\rangle$ vs. the averaged solar wind speed, proton temperature, and plasma β. SFRs in ICMEs, SIRs, and background solar wind are shown in the first column, second column, and third column, respectively. In each panel, the horizontal dotted line represents that the mean value of $\langle Q_{\rm Fe}\rangle$ is 12.

3.2. Iron Average Charge States in SFRs

The iron charge states tend to "freeze-in" in the interplanetary space since the ionization and recombination timescales are larger than the solar wind ion expansion time. Therefore, the existence of the high iron charge state ($\langle Q_{\rm Fe}\rangle > 12$) is an effective indicator of a flare-related heating process. In that case, it is a wise choice to determine the origin of SFRs by analyzing the averaged charge state of iron in them.

The iron charge states are obtained from the Solar Wind Ion Composition Spectrometer (SWICS) on board ACE, which gives the elemental abundance, charge state composition, and kinetic properties of heavy ions in the solar wind. Data before 2011 August 23 are obtained from SWICS 1.1, and have a time resolution of 1 hr. Data after that time are from SWICS 2.0, and have a time resolution of 2 hr. Since the time resolutions of the data are very low, it is hard for us to analyze the distribution of $\langle Q_{\rm Fe}\rangle$ in SFRs with a short duration. So in this section, we only focus on SFRs that last more than 3 hr. After such a selection, only 260 SFRs$_{\rm ICME}$, 250 SFRs$_{\rm SIR}$, and 1024 SFRs$_{\rm SW}$ are left.

Figure 2 shows an example of the SFR with high $Q_{\rm Fe}$ on 2000 November 7. From the top to the bottom, the panels are the averaged iron charge state ($\langle Q_{\rm Fe}\rangle$), the bulk speed of the solar wind ($V_{\rm bulk}$), three components of the solar wind speed (V_x, V_y, V_z) in GSE coordinates, the magnitude of the total magnetic field ($B_{\rm total}$), three components of the magnetic field (B_x, B_y, B_z) in GSE coordinates, proton temperature ($T_{\rm p}$), proton density ($N_{\rm p}$), and plasma β. The orange shaded region represents the SFR interval. This SFR is located in an ICME ejecta (the interval between the two blue vertical dashed lines), which clearly shows the signatures of enhanced magnetic field strength, large and smooth rotation of the magnetic field vector, lower than expected proton temperature, as well as low proton density and β. This ICME is fast and strong, so it drives a fast forward shock (the violet vertical dashed line) with a speed of 620 km s^{-1} and a density compression ratio of 2.4. In this SFR, $\langle Q_{\rm Fe}\rangle$ peaked at 8:17 on 2000 November 7 with the value of 14.6, and during the whole SFR interval, the mean value of $\langle Q_{\rm Fe}\rangle$ is 12.4. In addition, this SFR is not the only one in the ICME, there are also six small SFRs that last less than 3 hr, which are indicated by gray shaded regions. Since in this section we only focus on the SFRs longer than 3 hr, they are not studied.

Figure 3 shows the two-dimensional distribution of mean value of $\langle Q_{\rm Fe}\rangle$ in the SFRs versus the averaged solar wind speed, $\langle V_{\rm sw}\rangle$, proton temperature, $\langle T_{\rm p}\rangle$, and plasma β, $\langle\beta\rangle$. SFRs in ICMEs, SIRs, and background solar wind are shown in the first column, second column, and third column, respectively. In each panel, the color bar represents the number of SFRs. And the black line indicates that $\langle Q_{\rm Fe}\rangle$ equals 12, which is the

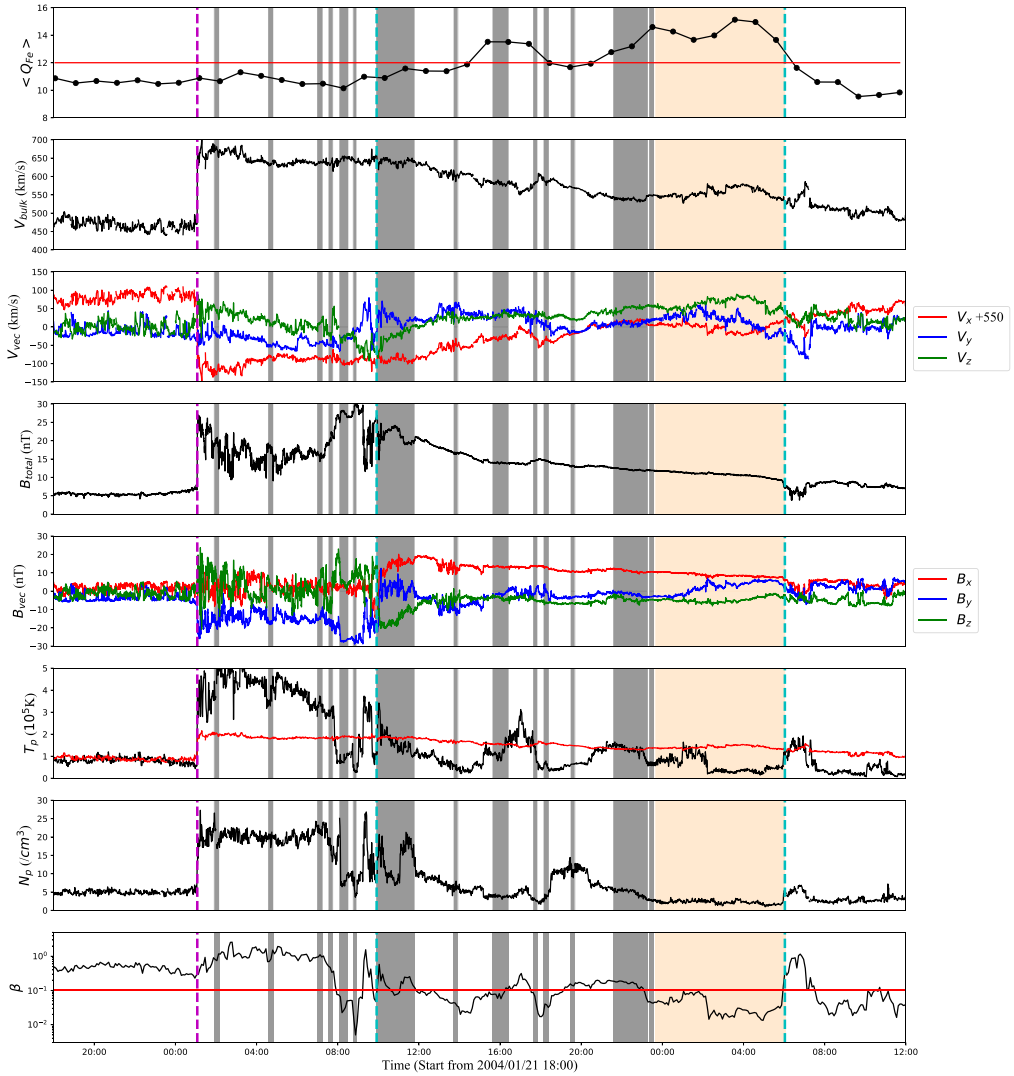

Figure 4. An example of the SFR with high $Q_{\rm Fe}$ on 2004 January 22. From the top to the bottom, the panels are the averaged iron charge state ($\langle Q_{\rm Fe}\rangle$), the bulk speed of the solar wind ($V_{\rm bulk}$), *x, y, z* components of the solar wind speed (V_x, V_y, V_z) in GSE coordinates, the magnitude of the total magnetic field ($B_{\rm total}$), *x, y, z* components of the magnetic field (B_x, B_y, B_z) in GSE coordinates, proton temperature ($T_{\rm p}$), proton density ($N_{\rm p}$), and proton β. The orange shaded region represents the studied SFR. The gray shaded regions represent the other SFRs in the suspected ICME event. The violet vertical dashed line is the shock time, and the following two cyan vertical dashed lines mark the possible ICME ejecta.

threshold for the high iron charge state. From this figure, we can find that most of the SFRs have a mean $\langle Q_{\rm Fe}\rangle$ in the range of [9, 11], which is the typical iron charge state in the solar wind. Only a few SFRs have high $Q_{\rm Fe}$ ($\langle Q_{\rm Fe}\rangle$ >12), and the majority of them have low β and low proton temperature, which are also the characteristics of MCs. Actually, only 155 SFRs are found to have a mean $\langle Q_{\rm Fe}\rangle$ greater than 12, accounting for 12% of the total. Among these SFRs with high iron charge states, 93 are SFRs$_{\rm ICME}$, 3 are SFRs$_{\rm SIR}$, and 59 are SFRs$_{\rm SW}$. The probability of high iron charge states in SFRs$_{\rm ICME}$ is 36%, which is much higher than that of SFRs$_{\rm SIR}$ (1%) and SFRs$_{\rm SW}$ (6%). Adopting the high iron charge state as an indicator of SFRs originating from the solar eruption, we find that it is appropriate to assume that SFRs$_{\rm ICME}$ and MCs have the same origin. Meanwhile, most of the SFRs$_{\rm SIR}$ and SFRs$_{\rm SW}$ are not produced by flare-related solar eruptions.

In addition, Figure 4 shows an example of SFRs$_{\rm SW}$ with a high iron charge state. The layout of it is the same as Figure 2. In this SFR, which is shown by the orange shaded region, $\langle Q_{\rm Fe}\rangle$ is always higher than 12 and reaches a maximum of 15.3 in the middle. Twenty-two hours ahead of this SFR, there is a strong shock with a velocity of 730 km s^{-1} and a density compression ratio of 3.2. Such a strong shock is most likely to be driven by an ICME. Therefore, it is highly possible that this SFR is actually located in an ICME. Since ICMEs are more narrow than the shocks they drive and they can be contaminated by the background solar wind during the propagation, it is common to see shocks without a clear CME driver at 1 au. In this case, the ICME is still vaguely recognizable, which is marked by the two cyan vertical dashed lines. In it, we can see the decreasing solar wind speed, slightly enhanced magnetic field strength, smooth rotation of the magnetic field vector, lower than expected proton temperature, and relatively low β. Again, the gray shaded regions in this suspected ICME are the SFRs with a duration less than 3 hr. They are not studied in this section. There are many similar cases. Of the 59 SFRs$_{\rm SW}$ with high $\langle Q_{\rm Fe}\rangle$, 9 have fast forward shocks within 24 hr in front of them and 17 have fast forward shocks within 36 hr in front of them. Considering that the occurrence rate of fast forward shocks at 1 au is relatively low, with about 60 per year at solar maximum

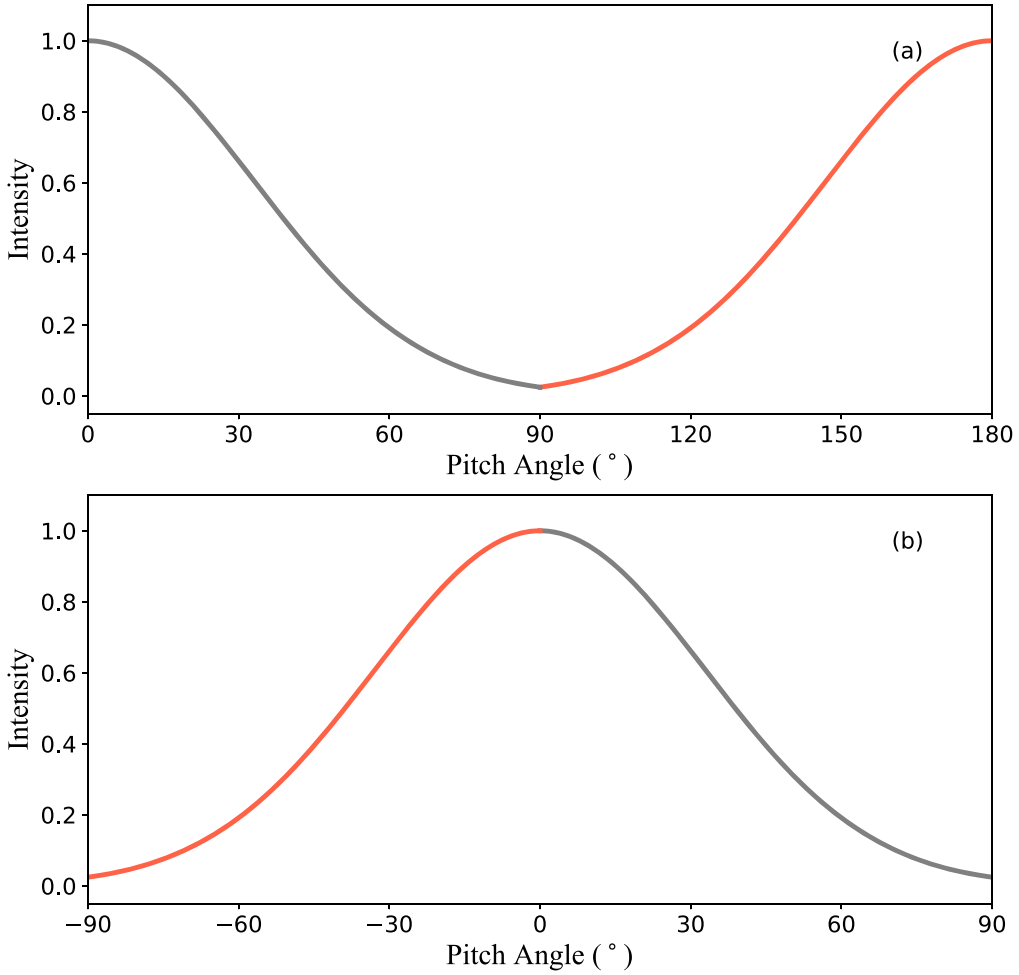

Figure 5. Schematic figure to illustrate the transformation of the pitch angle. In panel (b), the pitch angles of electrons between 90° and 180° are reduced by 180°.

and about 10 per year at solar minimum, we think that some $SFRs_{SW}$ are in fact $SFRs_{ICME}$. This suggests that the occurrence rate of a high iron charge state should be even lower in real $SFRs_{SW}$. So it is reasonable to assume that $SFRs_{SW}$ have a different origin from MCs.

Feng & Wang (2015) have surveyed the high iron charge states in 24 SFRs from 1998 to 2005. Unlike us, they used the maximum rather than mean values of $\langle Q_{Fe} \rangle$ in SFRs as a marker to see if they have high iron charge states. They found that as high as 50% of the SFRs contain enhanced iron charge states. In their 24 SFRs, 15 are partially or entirely located in ICMEs, with only 9 SFRs located in other types of solar wind. For the 15 SFRs located in ICMEs, 11 have high $\langle Q_{Fe} \rangle$, accounting for 73%. For the 9 SFRs located outside ICMEs, two have high $\langle Q_{Fe} \rangle$, accounting for 22%. To some extent, their results are consistent with ours: SFRs in ICMEs are more likely to have high $\langle Q_{Fe} \rangle$ than SFRs outside ICMEs, although their ratios are higher. The discrepancy between our results may be due to the different events and the criteria for a high iron charge state. Therefore, following their approach, we reanalyze our database using their method by focusing on the maximum of $\langle Q_{Fe} \rangle$ in SFRs from 1998 to 2005. In this case, 65% and 13% of SFRs in and outside ICMEs are found to have high $\langle Q_{Fe} \rangle$, which is much closer to their results. On the other hand, Yu et al. (2014) analyzed 549 SFRs with durations from 0.5 hr to 12 hr observed by STEREO-A from 2007 to 2014, finding that only 5% have enhanced $\langle Q_{Fe} \rangle$. However, in their study, SFRs located in ICMEs are eliminated, so the statistical results are only for the SFRs outside ICMEs. Hence, it seems that our results are pretty much in line with theirs.

3.3. Counterstreaming Suprathermal Electrons in SFRs

Counterstreaming suprathermal electrons are another important indicator to determine the origin of SFRs. SFRs with apparent CSEs mean that they are still attached to the solar surface, and can therefore be considered to have originated from the solar eruptions. However, CSE intervals are usually identified by naked eye in previous studies, which may be relatively subjective. In order to determine the proportion of CSE intervals in SFRs more accurately, we develop a method to automatically identify CSE intervals. Here, we also only focus on the SFRs longer than 3 hr. In this study, the suprathermal electrons are obtained from the Solar Wind Electron, Proton, and Alpha Monitor (SWEPAM) on the ACE spacecraft. The electrons are measured by SWEPAM at 20 pitch angle (PA) bins, covering 0°–180°. These suprathermal electron data are collected with a cadence of 128 s before 1999 September 23, and 64 s after that date. Here, we choose to analyze the pitch angle distributions (PADs) of 272 eV electrons.

To objectively quantify whether electron PADs include counterstreaming strahls, we devise the following algorithm. We divide the electron PADs into two halves: electron PADs

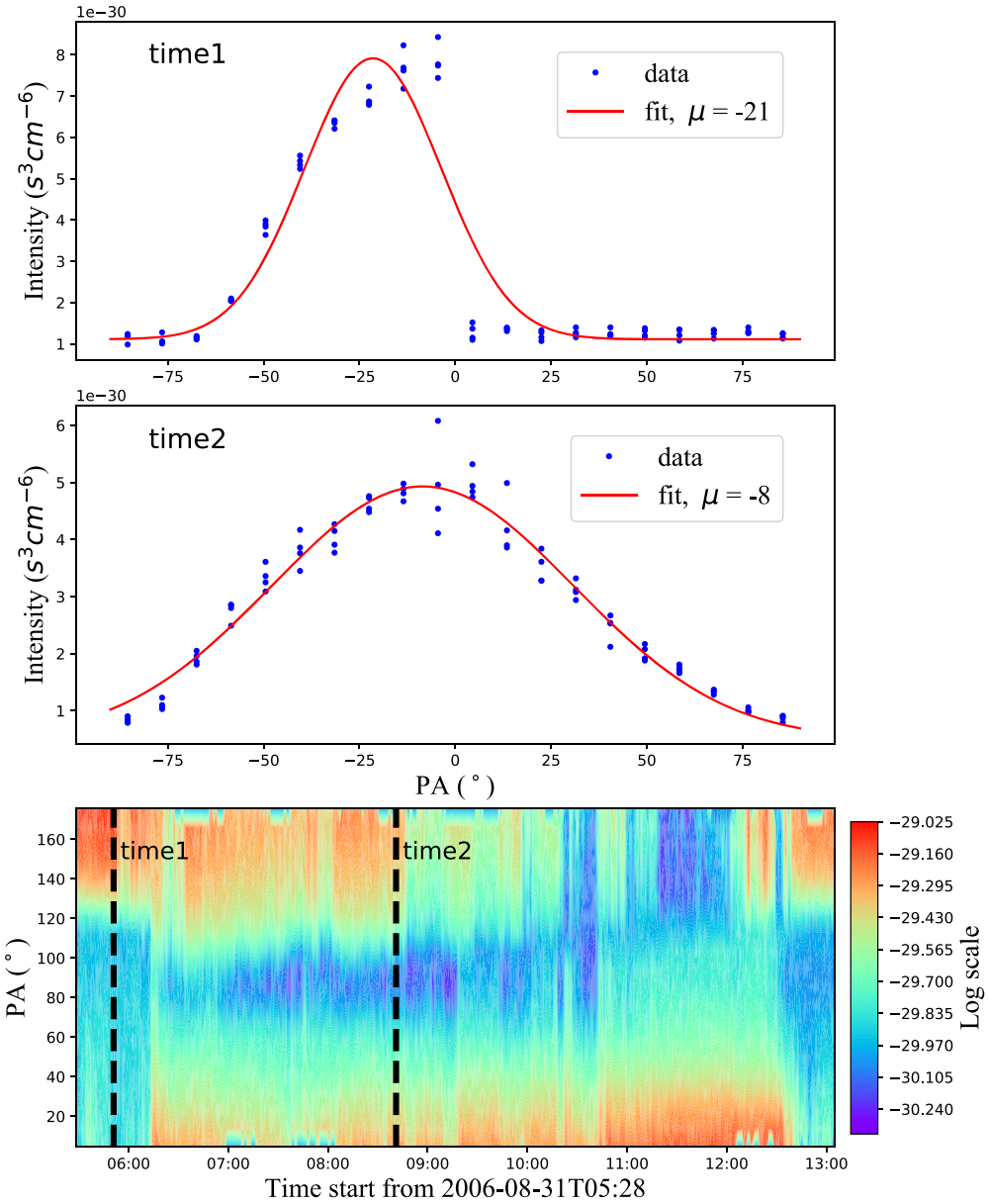

Figure 6. An example of of the method of determining the counterstreaming suprathermal electron signature.

with PAs from 0° to 90° and from 90° to 180°. For electrons with PAs between 90° and 180°, we subtract 180° from their PA. In this way, the PAs come to range from −90° to 90°. Figure 5 shows this transformation method. Through this transformation, the PADs of counterstreaming suprathermal electrons can be regarded to obey a Gaussian distribution centered around 0° (Anderson et al. 2012). For each SFR event, we average the PAD data every 10 minutes. We require that at least 70% of PAD data points should be nonzero. If not, the PAD data at that moment will be discarded. Then the PAD data will be substituted into the Equation (1) for fitting:

$$F(\theta) = A_0 e^{\frac{-(\theta-\mu)^2}{2\sigma^2}} + A_1. \quad (1)$$

In Equation (1), $F(\theta)$ is the particle density as a function of PA, A_0 is the Gaussian amplitude, μ is the PA offset of the center of the Gaussian, σ is proportional to the width of the Gaussian, and A_1 is a constant term. I, we define the width of the Gaussian (W) as the half-width at half-maximum of the entire fit function (Equation (2)). If the PAD satisfy the following criteria: (1) $A_0 > 0$, (2) $|\mu| < 15$, (3) $\Delta\mu < 10$, and (4) $10° < W < 80°$, we believe that there exists obvious CSEs. For each SFR, we follow the above procedure at each moment to determine the proportion of the region with obvious CSEs:

$$W = |\sigma|\sqrt{-2\ln\frac{(A_0 - A_1)}{2A_0}}. \quad (2)$$

Figure 6 shows an example. The bottom panel is the PADs of 272 eV electrons. From it, we select two moments: time1 and time2. As can be seen by the naked eye, the PADs at time1 and time2 are unidirectional and counterstreaming, respectively. By substituting the data near these two moments into the above procedure, we get the first two panels, in which the horizontal axis represents the transformed PA and the vertical axis represents the electron intensity. In each panel, the blue dots represent observational data, and the red curve represents the fitting result. At time1, the Gaussion distribution centers at

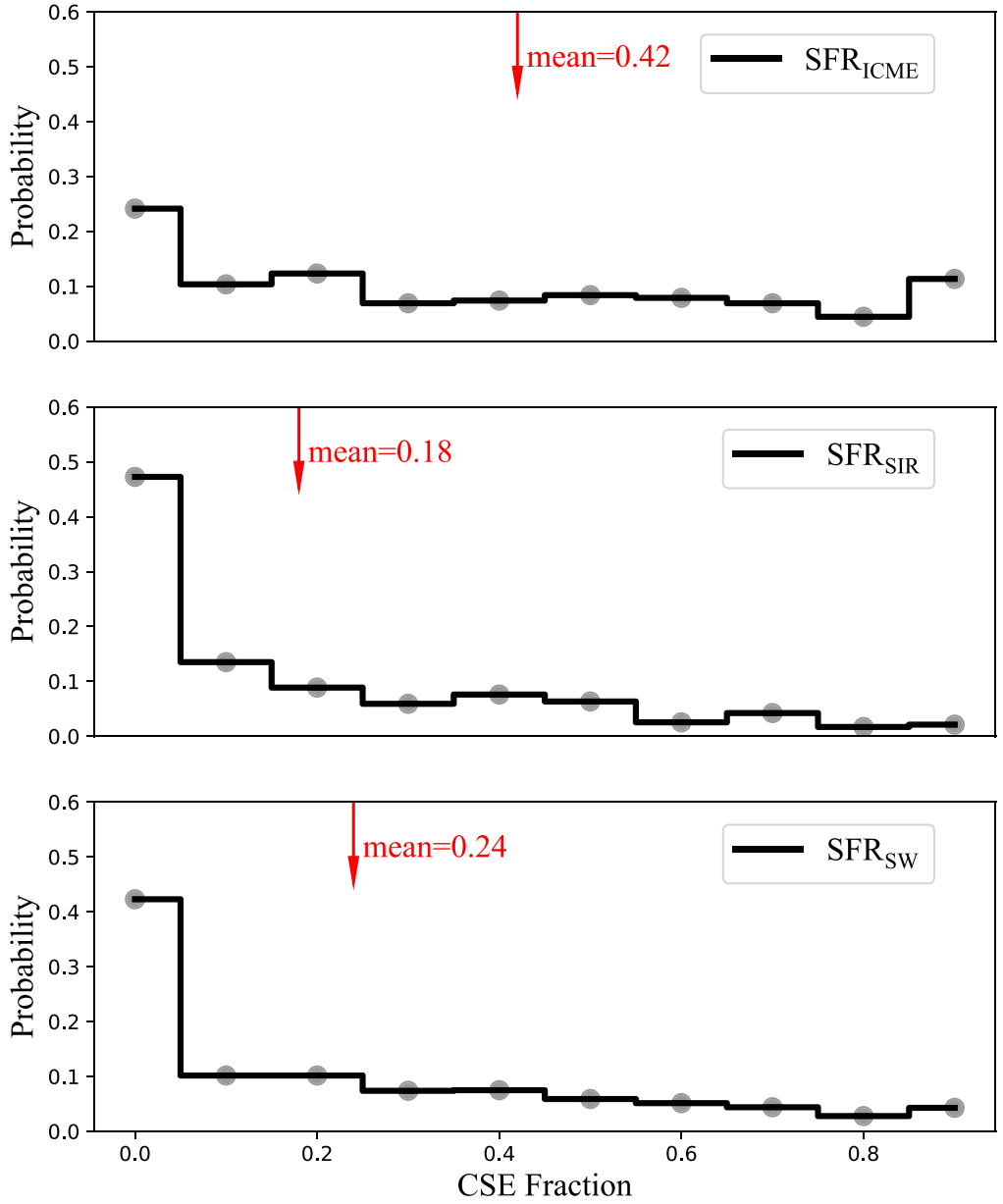

Figure 7. Distribution of CSE fractions in different types of SFRs. The horizontal axis represents the ratio of the CSE length to the SFR length, and the ordinate is the probability. On average, the duration of CSE accounts for 0.42, 0.18, and 0.24 of the total duration of SFRs$_{ICME}$, SFRs$_{SIR}$, and SFRs$_{SW}$, respectively.

$-21°$, while at time2, it centers at $-8°$. So time2 can be regarded as a CSE period.

Figure 7 shows that the CSE intervals account for 42%, 18%, and 24% of the total duration of SFRs$_{ICME}$, SFRs$_{SIR}$, and SFRs$_{SW}$, respectively. The signature of CSEs is more remarkable in SFRs$_{ICME}$ than in the other two groups of SFRs. Anderson et al. (2012) have calculated the fractions of time that counterstreaming electrons were observed in the solar wind from 1998 to 2015 as well as in the ICMEs from Cane & Richardson (2003) and Jian et al. (2006), finding that roughly one-third of ICME intervals show counterstreaming as compared to 10% of the solar wind as a whole. By comparing their results, we conclude that SFRs$_{ICME}$ display a high range of CSE, which is similar to ICMEs. Therefore, they may remain connected to the Sun at 1 au. For SFRs$_{SIR}$ and SFRs$_{SW}$, the CSE intervals are much smaller. This may suggest a different origin or different evolutionary processes for SFRs outside ICMEs.

4. Summary of the Results and Conclusions

Based on the database of SFRs with a duration from 9 minutes to 36 hr developed by Chen et al. (2019) through an automated detection algorithm, together with the ICME and SIR catalogs that we recently established, in this work we studied the properties of the SFRs in different types of solar wind, i.e., SFRs in ICMEs (SFRs$_{ICME}$), SFRs in SIRs (SFRs$_{SIR}$), and SFRs in background solar wind (SFRs$_{SW}$). Supposing that SFRs$_{ICME}$ originate from the solar eruption, we compare SFRs$_{ICME}$ with SFRs$_{SIR}$ and SFRs$_{SW}$ from the perspectives of basic characteristics, iron charge state, and counterstreaming suprathermal electrons, trying to find the origin of SFRs outside the ICMEs. The main findings of this paper are as follows:

1. Only 9% of the SFRs are located in ICMEs. Most of the SFRs are in the background solar wind and SIRs.

2. $SFRs_{SIR}$ and $SFRs_{SW}$ seldom have the signatures of large magnetic field strength and apparent expansion, which are otherwise common in MCs.
3. Only 12% of SFRs shows the feature of enhanced iron charge states, which is related to flare heating. The probability of high iron charge states in $SFRs_{ICME}$ is 36%, which is 6 times and over 30 times higher than those of $SFRs_{SIR}$ and $SFRs_{SW}$, respectively.
4. The presence of CSEs in $SFRs_{ICME}$ is more common. The duration of CSEs accounts for 42%, 18%, and 24% of the total duration of $SFRs_{ICME}$, $SFRs_{SIR}$, and $SFRs_{SW}$, respectively.

From all of these findings, we conclude that most of the SFRs detected at Earth have a different origin from MCs, presumably formed in the interplanetary space (see, e.g., Zheng & Hu 2018).

The authors are grateful to the referee for many helpful comments. We acknowledge the use of data resources from the ACE and Wind mission, and National Space Science Data Center, and National Science & Technology Infrastructure of China (http://www.nssdc.ac.cn). This work is supported by grants from the Strategic Priority Program of CAS (XDB41030100), NSFC (42004143, 41822405,41774181 41774178, 41904151), the Fundamental Research Funds for the Central Universities (WK2080000140, WK2080000122), Project funded by China Postdoctoral Science Foundation (2019M652194), and Anhui Provincial Natural Science Foundation (1908085MD107).

ORCID iDs

Qiang Hu https://orcid.org/0000-0002-7570-2301
Yuming Wang https://orcid.org/0000-0002-8887-3919
Yutian Chi https://orcid.org/0000-0001-9315-4487

References

Anderson, B. R., Skoug, R. M., Steinberg, J. T., & McComas, D. J. 2012, JGRA, 117, A04107
Bemporad, A., Poletto, G., Suess, S. T., et al. 2006, ApJ, 638, 1110
Buergi, A., & Geiss, J. 1986, SoPh, 103, 347
Burlaga, L., Sittler, E., Mariani, F., & Schwenn, R. 1981, JGR, 86, 6673
Cane, H. V., & Richardson, I. G. 2003, JGRA, 108, 1156
Cartwright, M. L., & Moldwin, M. B. 2008, JGRA, 113, A09105
Cartwright, M. L., & Moldwin, M. B. 2010, JGRA, 115, A08102
Chen, Y., Hu, Q., & le Roux, J. A. 2019, ApJ, 881, 58
Chi, Y., Shen, C., Luo, B., Wang, Y., & Xu, M. 2018, SpWea, 16, 1960
Chi, Y., Shen, C., Wang, Y., et al. 2016, SoPh, 291, 2419
Feng, H. Q., & Wang, J. M. 2015, ApJ, 809, 112
Feng, H. Q., Wu, D. J., & Chao, J. K. 2007, JGRA, 112, A02102
Feng, H. Q., Wu, D. J., Lin, C. C., et al. 2008, JGRA, 113, A12105
Feng, H. Q., Zhao, G. Q., & Wang, J. M. 2015, JGRA, 120, 10,175
Hu, Q., Zheng, J., Chen, Y., le Roux, J., & Zhao, L. 2018, ApJS, 239, 12
Hu, S. Q. 2017, ScChD, 60, 1466
Huang, J., Liu, Y. C. M., Peng, J., et al. 2018, JGRA, 123, 7167
Janvier, M., Démoulin, P., & Dasso, S. 2014a, SoPh, 289, 2633
Janvier, M., Démoulin, P., & Dasso, S. 2014b, JGRA, 119, 7088
Jian, L., Russell, C. T., Luhmann, J. G., & Skoug, R. M. 2006, SoPh, 239, 393
Ko, Y.-K., Raymond, J. C., Rakowski, C., & Rouillard, A. 2013, in AIP Conf. Ser. 1539, Solar Wind 13, ed. G. P. Zank et al. (Melville, NY: AIP), 207
Larson, D. E., Lin, R. P., McTiernan, J. M., et al. 1997, GeoRL, 24, 1911
Lepping, R. P., Jones, J. A., & Burlaga, L. F. 1990, JGR, 95, 11957
Lepri, S. T., & Zurbuchen, T. H. 2004, JGRA, 109, A01112
Lepri, S. T., Zurbuchen, T. H., Fisk, L. A., et al. 2001, JGR, 106, 29231
Moldwin, M. B., Ford, S., Lepping, R., Slavin, J., & Szabo, A. 2000, GeoRL, 27, 57
Moldwin, M. B., Phillips, J. L., Gosling, J. T., et al. 1995, JGR, 100, 19903
Nieves-Chinchilla, T., Jian, L. K., Balmaceda, L., et al. 2019, SoPh, 294, 89
Richardson, I. G., & Cane, H. V. 1995, JGR, 100, 23397
Song, H., & Yao, S. 2020, ScChE, 63, 2171
Song, H. Q., Chen, Y., Zhang, J., et al. 2015, ApJL, 808, L15
Yu, W., Farrugia, C. J., Galvin, A. B., et al. 2016, JGRA, 121, 5005
Yu, W., Farrugia, C. J., Lugaz, N., et al. 2014, JGRA, 119, 689
Zheng, J., & Hu, Q. 2018, ApJL, 852, L23